JACS
JOURNAL OF THE AMERICAN CHEMICAL SOCIETY
Article
pubs.acs.org/JACS

CO Oxidation on Au/TiO_2: Condition-Dependent Active Sites and Mechanistic Pathways

Yang-Gang Wang,[†] David C. Cantu,[†] Mal-Soon Lee,[†] Jun Li,[‡] Vassiliki-Alexandra Glezakou,[†] and Roger Rousseau*[,†]

[†]Institute for Interfacial Catalysis, Pacific Northwest National Laboratory, Richland, Washington 99354, United States
[‡]Department of Chemistry, Tsinghua University, Beijing 100084, China

Supporting Information

ABSTRACT: We present results of ab initio electronic structure and molecular dynamics simulations (AIMD), as well as a microkinetic model of CO oxidation catalyzed by TiO_2 supported Au nanocatalysts. A coverage-dependent microkinetic analysis, based on energetics obtained with density functional methods, shows that the dominant kinetic pathway, activated oxygen species, and catalytic active sites are all strongly depended on both temperature and oxygen partial pressure. Under oxidizing conditions and T < 400 K, the prevalent pathway involves a dynamic single atom catalytic mechanism. This reaction is catalyzed by a transient Au—CO species that migrates from the Au-cluster onto a surface oxygen adatom. It subsequently reacts with the TiO_2 support via a Mars van Krevelen mechanism to form CO_2 and finally the Au atom reintegrates back into the gold cluster to complete the catalytic cycle. At 300 ≤ T ≤ 600 K, oxygen-bound single O_{ad}—Au^+—CO sites and the perimeter Au-sites of the nanoparticle work in tandem to optimally catalyze the reaction. Above 600 K, a variety of alternate pathways associated with both single-atom and the perimeter sites of the Au nanoparticle are found to be active. Under low oxygen pressures, O_{ad}—Au^+—CO species can be a source of catalyst deactivation and the dominant pathway involves only Au-perimeter sites. A detailed comparison of the current model and the existing literature resolves many apparent inconsistencies in the mechanistic interpretations.

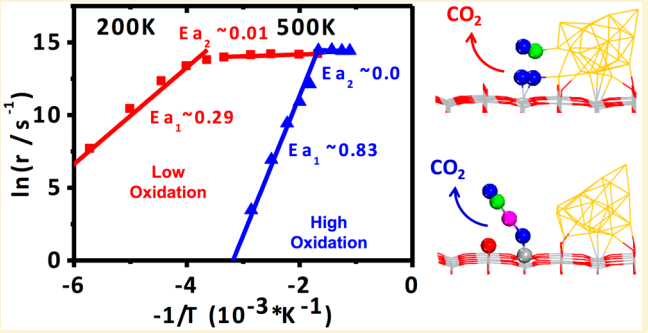

INTRODUCTION

A fundamental issue that has plagued the catalysis literature for over a century is the question of what is the actual active species under operating conditions.[1−3] Detection of active species is elusive because they are formed under reaction conditions, are short-lived and in low abundance, making their unambiguous detection and identification difficult.[4−7] It is well-known that catalytic nanoparticles adapt their size, shape, surface coverage, and even composition under different reactive conditions.[8−10] Against this backdrop, there is a lively debate about the role of single metal atoms.[11−17] Our current ability to detect these species either in situ or ex situ[11,18−21] has led many authors to speculate that, in some instances, single metal atoms may in fact be the active catalytic agents. An additional level of complexity is introduced by evidence that reaction mechanisms and pathways change with temperature, reactant concentrations (partial pressures) and identity of surface bound species.[22−28] However, much less is understood regarding the influence of chemical environment on the nature of the active sites. Theoretical simulations have done much to advance our understanding of catalytic conversions, but often rely on simplistic models of the active catalytic sites, and rarely address how these may change under operating conditions. Advances in computational methodologies have allowed us to address more complex models of catalyst reactivity and discovered new mechanistic routes that elucidate the principles of reactivity in complex environments.[22,29−34] In the current paper, we discuss the variation of active catalytic sites and mechanistic routes under different reaction conditions by means of large scale ab initio molecular dynamics simulations and microkinetic modeling. We illustrate these points using a prototypical model reaction: CO oxidation on TiO_2 supported Au clusters. Given the abundance of experimental literature and the hotly debated topic, this study will serve to both validate our model and resolve existing controversies. We will demonstrate the variation of active catalytic sites and mechanistic details as a function of operating conditions.

Nanosized Au particles supported on metal oxides have been extensively studied because of their high reactivity in a variety of important catalytic reactions.[35−40] Low temperature CO oxidation on TiO_2 supported Au nanocatalysts is a typical model system used to elucidate the chemical nature of gold catalysis.[41−44] Even though a series of CO oxidation reaction mechanisms have been proposed at atomic resolution, several fundamental issues remain unsettled. First, the type of active

Received: April 24, 2016
Published: August 2, 2016

DOI: 10.1021/jacs.6b04187
J. Am. Chem. Soc. 2016, 138, 10467−10476

oxygen species is still unclear. Oxygen adatoms, molecular O_2, and lattice oxygen ions have all been proposed as potential oxidative species in CO oxidation by different research groups.[45−54] For example, Green et al. recently proposed that CO oxidation occurs with O_2 via the formation of CO—O_2 complex at the perimeter of Au nanoparticles using IR spectroscopy and density functional theory (DFT) calculations.[52] Simultaneously, various theoretical calculations also identified the adsorbed molecular O_2 as the active oxygen species.[49−51,54,55] However, molecular O_2 desorption is observed at 170 K,[46] indicating that O_2 would not contribute to CO oxidation at relatively high temperatures. Furthermore, Widmann et al., reported that at $T > 353$ K the active oxygen species is either a highly stable atomic oxygen species that is present only at the perimeter of the Au−oxide interface, or a lattice oxygen ion.[41,53] Second, identifying the CO oxidation active site is challenging. Although it is generally accepted that CO oxidation proceeds around the perimeter of gold particles on the support,[35] perimeter site structural details are unclear due to experimental detection difficulties. Positively charged or low coordinated sites on gold particles at the interface have been proposed as the active site by many theoretical simulations,[56−58] while recent experiments (STM, FTIR) reveal that single gold sites linked to an oxygen atom in the interfacial area contribute to gold catalysis activity.[11]

Previously we reported that CO adsorption led to the strong reconstruction of gold particles and spontaneous formation of low coordinated sites and mobile Au—CO species.[29] Recent room-temperature STM experiments have demonstrated the mobile Au—CO species on gold surface and have thus confirmed our prediction.[19] Furthermore, we found that on CeO_2 supported gold nanocatalysts, the adsorption of CO can lead to the formation of a dynamic single-atom catalysis (DSAC) active site, which was attributed to the strong redox coupling of the single Au with the CeO_2 lattice.[31] This finding serves as motivation to ask if a dynamic site mechanism could occur on a TiO_2 support, which is much less oxidizing than CeO_2 and hence potentially not energetically viable compared with alternate pathways.

To date, two different reaction mechanisms for CO oxidation have been proposed by both experimental and theoretical studies: the Langmuir−Hinshelwood (LH) and Mars van Krevelen (MvK) mechanisms.[29,47,49−53,56,59,60] In the LH mechanism, the gold cluster bound CO is generally reported to react with adsorbed O_2 or O species at perimeter sites to produce CO_2. Recently, we presented a systematic analysis of this reaction mechanism.[29] We showed that the first CO oxidation by an adsorbed O_2^{2-}, does not change the redox state of the support/nanoparticle. Conversely, the second CO oxidation with the O adatom (O_{ad}) does affect the redox state. We also pointed out that the energetics of redox processes are strongly affected by availability of excess charge in the system. In the MvK mechanism, the CO on the Au cluster is reported to be oxidized by a lattice oxygen atom. This mechanism is theoretically predicted to occur only under oxidizing conditions where additional O_2 molecules or O atoms are adsorbed at the interfacial area.[41,47,53,60] Here we investigate whether or not a similar dynamic adatom mechanism is also possible on Au/TiO_2 and how this compares with other theoretical studies as well as available experimental literature.

Considering these complex observations, we set to resolve two questions: (i) How do reaction mechanisms and active sites affect each other and vary as a function of temperature and pressure? (ii) How does the oxidation condition of the system affect the nature of the active site and relevant reaction mechanisms? To answer these questions, we perform density functional theory (DFT) based ab initio molecular dynamics (AIMD) simulations to explore the reactivity and dynamics of TiO_2 supported Au catalysts in the CO oxidation reaction. We consider the dynamics of atoms in the Au metal particle, TiO_2 support, reactants and products, as well as the excess charge carriers within a reducible TiO_2 surface. We present a microkinetic model, based on ab initio electronic structure information, with five competing reaction pathways including those based on metal particles as well as single atoms. We demonstrate that all mechanisms are viable depending on the reaction conditions. Finally, we use this model to explain many seemingly disparate and potentially conflicting observations in the literature. Overall, we demonstrate that in order to understand the activity of single atoms catalysts, it is necessary to account not only for the complexity associated with multiple catalytic pathways, but also the change in catalytic sites under varying reaction conditions.

COMPUTATIONAL DETAILS

All calculations were performed using spin-polarized DFT methods as implemented in the QUICKSTEP code of the CP2K package.[61] The generalized-gradient approximation (GGA) with Perdew−Burke−Ernzerhof (PBE) functional was used to evaluate the exchange and correlation.[62] The wave functions were expanded in a molecularly optimized (MOLOPT) double-ζ Gaussian basis set[63] with a cutoff energy of 350 Ry. Core electrons were modeled by scalar relativistic norm-conserving pseudo potentials with 12, 6, 4, and 11 valence electrons of Ti, O, C, and Au, respectively.[64] The DFT+U method, with a U value of 13.6 eV, was used to describe the Ti 3d electrons. This value of U adopted was found to adequately reproduce the work function (W = 5.1 eV) and location of defect states at 1.2 eV below the conduction band of TiO_2. We point out that the large U value may affect the energy difference estimation for processes involving the direct transfer of excess 3d electrons, but will have only secondary effects on the processes occurring on Au_{20}/TiO_{2-x} because the excess charge is concentrated on the Au cluster; see extended discussion of the choice of U parameter included in the Supporting Information of our recent report.[29] Reaction path calculations were performed using the climbing image nudged-elastic-band method[65] (CI-NEB) including at least 9 replicas. The convergence criterion for the maximum force is set to 0.002 au.

A reduced rutile TiO_2(110)-p(6 × 3) surface slab with 4 O—Ti—O trilayers was used to model the TiO_2 substrate, where one bridging oxygen atom (O_b) is removed creating an oxygen vacancy (O_v). We kept the bottom O—Ti—O trilayer frozen during the simulations. The slab was repeated periodically with a vacuum thickness of ∼20 Å in the direction of the surface normal. A tetrahedral Au_{20} cluster placed over the O_v site was chosen to model Au particles. Details on the choice of model, its dynamical behavior and charge distribution in the Au_{20} /TiO_{2-x} system can be found in our recent study.[29]

Because of the easy O_2 dissociation and the reaction between *CO and *O_2, O_{ad} is expected to exist adjacent to the oxide metal interface. To account for the oxidation state of the surface under realistic conditions, we considered the Gibbs free energy of O_{ad} adsorption as a function of the oxygen chemical potential (μ_O), calculated as follows:[66]

$$\Delta G(T, P_i) \approx E_{N_O+Au/TiO_2} - E_{Au/TiO_2} - N_O\mu_O(T, p_i) \quad (1)$$

where $E_{NO+Au/TiO2}$ is the total energy of the Au/TiO_2 system with N_O, the number of O_{ad} at the interface, $E_{Au/TiO2}$ is the total energy of Au/TiO_2 surface without O_{ad}. Assuming equilibrium of the reaction 1/2 $O_2 \rightarrow O_{ad}$*, μ_O may be written as follows:

DOI: 10.1021/jacs.6b04187
J. Am. Chem. Soc. 2016, 138, 10467−10476

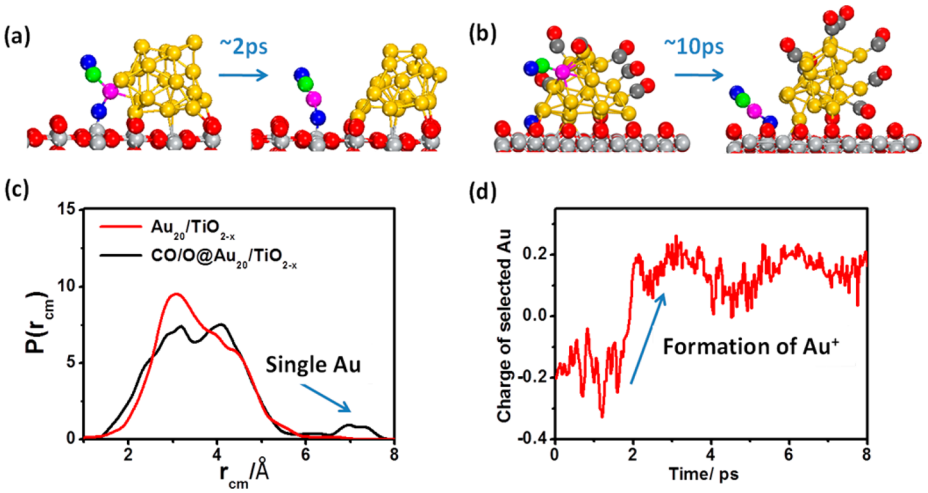

Figure 1. Initial and final configurations for 10 ps of AIMD simulation at 700 K with (a) one CO and one O_{ad}, and (b) 8 CO and 3 O_{ad}. (c) Distribution function $P(r_{cm})$ of Au atoms from the center of mass of the Au-nanoparticle. (d) Mulliken charge of isolated Au as a function of simulation time after equilibration. Color coding: C: green, O: blue and red, Ti: gray, and Au: gold and pink. For alternate perspective representations see Figure S3 as well as the supporting movie files.

$$\mu_O(T, p_i) = \mu_O(T, p^\phi) + \frac{1}{2}k_B T \ln\left(\frac{p_i}{p^\phi}\right) \quad (2)$$

where $\mu_O(T, p^o)$ is standard potential at p^o = 1 atm with its reference state μ_O (0 K, p^o) = 1/2 E_{O2} to be the total energy of oxygen in an isolated molecule at T = 0 K. We used values of $\mu_O(T, p^o)$ obtained from the previous study by Reuter et al.[66]

To account for the reaction kinetics of CO oxidation on Au/TiO_2 surface, a microkinetic model was constructed by numerically solving the differential equations that describe the coverage of all surface intermediates. All parameters were derived from DFT calculations. The rate constants of surface reactions and desorption steps were calculated using harmonic transition state theory by the following:[67−69]

$$k = \frac{k_B T}{h} e^{\Delta S/k_B} e^{-E_a/k_B T} \quad (3)$$

where k_B is the Boltzmann constant, and E_a is the calculated energy barrier. The energetics of the redox steps strongly depend on the oxidation state of the surface.[29] To account for the energetic dependence of the redox steps in the microkinetic modeling, a linear interpolation was used to obtain energy barriers at specific oxygen coverage by the following:

$$E_a = E_1 + \theta(E_2 - E_1) \quad (4)$$

where θ is the total coverage of all surface adsorbed oxygen species (O_{ad}, O_2* and covered O_{ad}), and E_1 and E_2 are the calculated energy barriers at reducing conditions (θ = 0) and oxidation conditions (θ = 1) respectively. In this way, our microkinetic model provides not only an appropriate description of the kinetics for the system at low and high oxidative conditions, but also an approximate estimation at conditions in between. The rate constant of adsorption was calculated by the following:

$$k = S \cdot P \cdot A / \sqrt{2\pi m k_B T} \quad (5)$$

where S, P, and A are the sticking coefficient, partial pressure of the adsorbed species, and the area of the adsorption site, respectively.[70] Here we assume S = 0.5 for all the species, which is a common value for small molecules such as O_2 and CO. Examination of S values from 0.1 to 1.0 showed no distinct difference in the kinetic results. We note that both the forward adsorption (eq 5) and reverse desorption (eq 3) steps are considered in order to account for the surface coverage of reactants in our kinetic model. A full breakdown of the parameters for all steps in our microkinetic models and discussion of the sensitivity of our results to variation in the parameters is provided in the Section S1 of the SI. In general, we find that the magnitude of reaction rates is sensitive, particularly at higher temperatures, but the trends in the prevalence of the preferred mechanistic route as a function of temperature are robust over variations in reaction energy barriers as large as 0.1 eV.

RESULTS

Formation of Interfacial Single-Atom Au Catalytic Sites. As discussed in our recent studies,[29,31] the dynamic behavior of catalysts under reaction conditions play a very important role in gold catalysis. Catalyst structural fluctuations and electronic properties strongly affect active site formation and reactant activation. Therefore, prior to considering any mechanistic details, it is necessary to understand how finite temperature and speciation influence the dynamic behavior of the catalyst under typical reaction conditions. Previous Fourier Transform Infrared (FTIR) spectroscopy experiments[71] have reported that the system exhibited a strong band at 2116 cm^{-1} under CO oxidation conditions which is attributed to a O—Au—CO species. Recently, Flytzani-Stephanopoulos et al.,[11] suggested that the actual active site on TiO_2 supported gold catalysts is a single Au site directly linked to a surface oxygen (O_{surf}). These implications inspired us to consider possible active sites for CO oxidation under oxidizing conditions.

We started our simulations with a well-equilibrated structure of the Au_{20}/TiO_2 system. AIMD simulations at 700 K were performed after adding a CO molecule onto the gold cluster and one oxygen adatom (O_{ad}) on a Ti_{5c} site at the periphery of the cluster (Figure 1a). The O_{ad} can be easily formed when CO reacts with an adsorbed O_2 molecule at the interface ($E_a \approx 0.3$ eV), or by dissociation of adsorbed O_2 ($E_a \approx 0.53$ eV). After 2 ps, we observed the dissociation of an Au—CO species from the gold cluster, followed by diffusion toward the O_{ad}. Additionally, to study the dynamic behavior in an unbiased way, a second AIMD simulation was performed after adding 8 CO molecules at random sites on the gold cluster and three O_{ad} at the interface. As shown in Figure 1b, an isolated O_{ad}—Au^+—CO species is formed through diffusion within the picosecond time scale. The function $P(r_{cm})$ (Figure 1c) is a measure of the probability distribution of an Au atom at a distance r_{cm} from the

DOI: 10.1021/jacs.6b04187
J. Am. Chem. Soc. 2016, 138, 10467−10476

center of mass of the Au_{20} nanoparticle. The isolated Au atom can be clearly identified by the peak at around ~7 Å in $P(r_{cm})$ indicated in Figure 1c. As the Au—CO unit breaks off from the cluster, the charge state of Au changes from negative (in the cluster) to positive (Figure 1d) indicating that, like on CeO_2,[31] the operative species is best thought of formally as an O_{ad}—Au^+—CO unit.

On our simulation time scale the Au—CO species moves freely on the cluster as was also shown in our previous studies.[29] On the contrary, once the O_{ad}—Au^+—CO forms at the perimeter of the cluster, it spends the remaining time of the trajectory at the same spot indicating a more stable species. This speculation regarding its stability was confirmed with free energy calculations, using the Blue Moon ensemble method (see Figure S4 for details), for the formation of the O_{ad}—Au^+—CO site which show the species as being favorable in free energy by −0.34 eV at 300 K. On the basis of the equilibrium constant estimation using $k_{eq} = \exp(-\Delta G/k_B T)$, the relative population of exposed O_{ad} vs O_{ad}—Au^+—CO sites is $1:10^6$. We note that the O_{ad}—Au^+—CO site is not fully isolated from the Au nanoparticle. It shows a transient Au—Au contact with the cluster on the order of ~3.0 Å ~ 40% of time as evident in the Au—Au radial distribution function shown in Figure S5a. The rapid formation of O_{ad}—Au^+—CO and its high stability indicate that, at low temperature, the presence of O_{ad} sites at the interface may not result in CO_2 production from cluster bound CO which is estimated to have a barrier of 0.3−0.7 eV, higher than that from formation of the O_{ad}—Au^+—CO.[29]

We next consider the mobility and stability of O_{ad}—Au^+—CO at the interfacial area. We find that the O_{ad}—Au^+—CO species does not diffuse to the adjacent bridging oxygen, O_b, sites or unsaturated surface titanium, Ti_{5c}, sites. Instead, the Au—CO atoms adsorbed on either O_b or Ti_{5c} sites slip back to the O_{ad} site spontaneously during a geometry optimization, as shown in Figure S6. This is estimated to be energetically favorable by at least ~1.0 eV for the Au—CO atoms to reside at O_{ad} sites than O_b or Ti_{5c} sites. Additionally, the energy barrier of O_{ad}—Au^+—CO diffusion along Ti_{5c} sites is estimated at 1.38 eV. This indicates the process to be slow at ambient conditions, but could still occur at higher temperatures. Thus, O_{ad}—Au^+—CO is anchored adjacent to the nanocluster/oxide interface.

Reactive Mechanisms for CO Oxidation. Given the above results we ask whether or not O_{ad}—Au^+—CO is active toward CO oxidation, or thermodynamically stable, hence potentially a step toward catalyst deactivation as has been debated in the literature.[72−74] Two major CO oxidation mechanisms have been previously proposed. In the LH mechanism, the first CO molecule on the gold cluster reacts with the adsorbed O_2 to produce the first CO_2 molecule, leaving one O_{ad} at the metal/oxide interface. A second CO molecule reacts with O_{ad} to produce the second CO_2, completing the catalytic cycle. However, as pointed out above, the second CO may form O_{ad}—Au^+—CO, thus hindering the second half cycle of the LH mechanism. Note, however, all reported energy barriers are 0.3−0.6 eV for CO oxidation,[29] as well as that for the back reaction to uncover the O_{ad} and reintegrate the Au—CO into the Au-nanoparticle. This indicates that temperature will have a critical effect upon the competition between these two processes.

In the MvK mechanism,[47] the first CO molecule on the gold cluster reacts with an O_b site, forming CO_2 and creating an O_v site. An O_2 molecule then fills the O_v site and a second CO reacts with the adsorbed O_2, completing the catalytic cycle. However, our AIMD simulations have shown that as soon as O_v is created, the Au cluster will extrude an Au atom to occupy the vacancy site, which hinders further O_2 adsorption, see Figure S7. The Au atom at the O_v site is extremely stable and does not move out of the vacancy even after 40 ps of AIMD simulation. An energy barrier of 1.90 eV was calculated for the O_{ad} on the surface to fill in the oxygen defect site and displace the gold atom, see Figure S7. The high-energy barrier suggests that surface bound O_{ad} replacing Au and completing the MvK catalytic cycle may not be operative at low temperatures. This realization requires a new mechanism to explain the experimental observation[41,53] that lattice oxygen atoms participate in CO oxidation under highly oxidizing conditions.

As discussed above, when O_{ad} adsorbs on Ti_{5c} sites, an Au—CO species can easily move from the cluster to form O_{ad}—Au^+—CO. Although this prevents further O_2 activation at the Ti_{5c} site, we investigated whether the CO at this site could react with the nearest lattice oxygen, O_b. On the basis of the amount of adsorbed oxygen, the TiO_2 oxidizing strength will vary. At low oxidizing conditions, with no extra O_{ad} except those within O_{ad}—Au^+—CO, we find that the energy barrier to extract O_b and form CO_2 is endothermic by 1.46 eV and a barrier of 2.47 eV. The red line in Figure 2b shows this reaction path. This

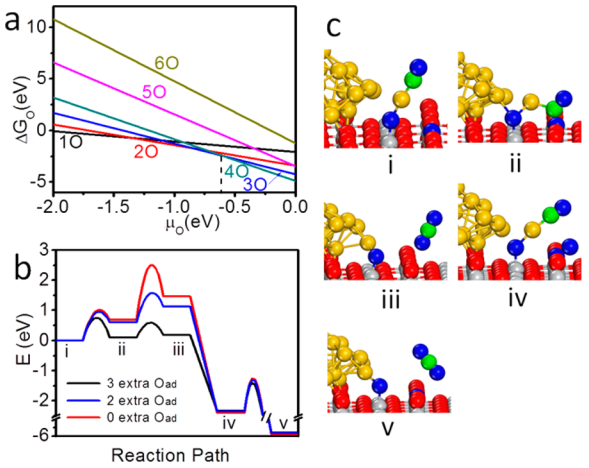

Figure 2. (a) Gibbs free energy of oxygen adsorption as a function of the chemical potential (μ_O) determined from eq 1, for different number of adsorbed oxygen atoms. (b) Energy diagram of CO oxidation mechanism at O_{ad}—Au^+—CO site under different oxidation states with 0, 2, or 3 extra O_{ad} on Ti_{5c} site (i.e., 1, 3, 4 O_{ad} on the surface). Energy unit of given values is eV. Color coding: C: green, O: blue and red, Ti: gray, and Au: gold and pink.

points to that, at low oxidizing conditions, the isolated Au site has little reactivity for CO oxidation and is potential source of catalyst deactivation.

Because of easy O_2 dissociation and the low energy barrier for CO reacting with the adsorbed O_2, an appreciable number of O_{ad} sites are expected to exist at the metal/oxide interface under high O_2 partial pressures. For instance, Hammer et al., recently placed up to 12 O_{ad} at the interface of Au_{24}/TiO_2 to create extremely oxidizing conditions for CO oxidation.[75] To estimate the oxidation state of the surface at realistic conditions, we include 1−6 O_{ad} adsorbed at Ti_{5c} sites, and consider the Gibbs free energy of oxygen adsorption as a function of oxygen chemical potential, μ_O, as computed by eq 1 and reported in Figure 2a. The configuration with 4 O_{ad} on the surface is the

DOI: 10.1021/jacs.6b04187
J. Am. Chem. Soc. 2016, 138, 10467−10476

Table 1. Work Functions and Bader Charges of Au_{20}/TiO_{2-x} with 1−4 O_{ad} (i.e. 0−3 extra O_{ad}) Co-adsorbed

no. of O_{ad}	1	2	3	4
work function (eV)	5.4	5.6	5.8	6.4
Bader charges of O_{ad} (e^-)	−1.05	−1.05, −1.02	−0.99, −1.04, −1.01	−0.96, −0.96, −0.98, −0.65

Table 2. Energetics for Elementary Reaction Steps during CO Oxidation on TiO_2 Supported Au_{20} Nanoparticles[a,b]

	low ox.		high ox.	
elementary steps	E_a	E_{-a}	E_a	E_{-a}
R1. CO + # → CO#		0.81		0.82
R2. O_2 + * → O_2*		1.73		0.30
R3. CO# + O_2* → CO_2 + O_{ad}* + #	0.32	3.47	0.37	3.56
R4. CO# + O_{ad} * → CO_2 + * + #	0.28	1.02	0.72	2.23
R5. CO# + O_{ad} * → O_{ad}—Au^+—CO*	0.26	0.60	0.30	0.64
R6. O_{ad}—Au^+—CO* + O_b→ CO_2 + O_v + O_{ad}*	2.47	1.01	0.81	0.62
R7. O_2 + O_v→ O_2—O_v		2.70		1.37
R8. O_{ad}—Au^+—CO* + O_2— O_v→ CO_2 + O_b + O_{ad}*	0.87	4.36	0.62	4.15
R9. O_{ad}* + O_v→ *	0.25	2.43	0.22	1.96
R10. O_2* + * → 2O_{ad}*	0.53	2.16	0.77	1.65

[a]Activation energies are reported for low (low ox.) and high oxidation (high ox.) levels. [b]The values for R1−R4 are obtained from our previous reaction pathways (see Table1, Figure 10 and Figure S12 of ref 27). The adsorption steps R1, R2, and R7 are assumed to have no forward reaction barriers. The backward rate for CO_2 production steps as R3, R4, R6, and R8 are not considered since we assume the CO_2 will be removed immediately once it is produced. # denotes the perimeter site on Au cluster, * for the Ti_{5c} site at the interface, O_b for the lattice oxygen ion, and O_v for the oxygen vacancy.

most stable over a wide range of μ_O values from approximately −0.6 to 0 eV, corresponding to $\sim 10^{-6} \leq P_{O2} \leq 1$ atm at 300 K, or $\sim 10^{-2} \leq P_{O2} \leq 1$ atm at 500 K. This indicates that the surface with 4 O_{ad} would be the most favorable at high O_2 pressure conditions for our model surface.

Therefore, we create a surface model including three extra O_{ad} on Ti_{5c} sites and one as O_{ad}—Au^+—CO. With this highly oxidized surface model we find that the O_{ad}—Au^+—CO can perform CO oxidation via a dynamic MvK (DMvK) mechanism similar to the one we proposed on a CeO_2 support.[31] This mechanism and associated reaction energetics is shown in Figure 2b. The first CO easily attaches to the adjacent O_b site to form a bent OCO intermediate (Configuration *i* to *ii*). This occurs with an energy barrier of 0.81 eV (E_{a1}) that is far lower than the barrier associated with low oxidizing conditions. This intermediate must overcome an energy barrier of 0.49 eV (E_{a2}) to desorb CO_2 into the gas phase (Configuration *iii*). Simultaneously the single Au atom reintegrates back into the Au nanoparticle. Note the energy for the Au atom to occupy the newly created O_v site is uphill by 0.93 eV and hence not likely to occur. Instead, at high P_{O2}, a gas phase O_2 molecule can readily fill the O_v site with a favorable binding energy of −1.37 eV, forming a peroxo $(O_2)^{2-}$ species. Subsequently, another O_{ad}—Au^+—CO (*iii* to *iv* Figure 2) can react with the peroxo $(O_2)^{2-}$ species with a small energy barrier of 0.62 eV (E_{a3}), followed by a second CO_2 release. Again we find that once CO is removed, the single Au atom can fully reintegrate into the nanoparticle, indicating that the single site is only transiently formed during the catalytic process. In the proposed DMvK mechanism, the rate-limiting step is the oxidation of the first CO by an O_b site, with an energy barrier of 0.81 eV, indicating the potential for low temperature catalytic activity.

To evaluate the underlying reason for the increased activity under oxidizing conditions, we consider the work function of the surface and Bader charges of O_{ad} sites, as presented in Table 1. It is shown that as the number of O_{ad} increases the work function increases from 5.4 to 6.4 eV, confirming that the surface becomes a stronger oxidizing agent. This is further validated by the fact that increasing the number of O_{ad} from 1 to 4, both the barriers and reaction energies for O_{ad}—Au^+—CO reacting with O_b (i.e., the first CO oxidation) decrease, as shown in Figure 2b. Interestingly, with the fourth O_{ad} added onto the surface, the work function shows an increase of 0.6 eV, leading to significant decrease in the barrier for the first CO oxidation from 1.56 to 0.81 eV. This is attributed to the lower negative charge (0.65 *e*−) on the fourth O_{ad} compared to the charge (∼1.0 *e*−) on the other three O_{ad}. This implies that the O_{ad} sites are only partially valence-saturated at high O_{ad} coverage, creating a sink for excess electrons generated when an O_b is extracted from the TiO_2 lattice. Our results agree with recent theoretical studies[47,60] that show that the reactivity with O_b occurs only at highly oxidizing conditions.

Note, when the O_v is generated after the first CO oxidation, the surface O_{ad} (Configuration *iii* in Figure 2) can also diffuse into the O_v with a very small barrier of 0.22 eV. On the one hand, this step will decrease the amount of surface O_{ad} and subsequently the O_{ad}—Au^+—CO species. On the other hand, it can be considered to complete another catalytic cycle where (i) the first CO reacts with an adsorbed O_2 at the Au nanoparticle/oxide interface, as in the LH mechanism; (ii) the second CO reacts with the O_b via a O_{ad}—Au^+—CO site; and (iii) the O_{ad} fills the O_v. This is a hybrid LH/DMvK mechanism, denoted as LM, which employs both single atom and cluster perimeter sites as catalysts.

Microkinetic Analysis. As alluded above, the viability of cluster edge sites and O_{ad}—Au^+—CO sites to catalyze the CO-oxidation reaction will have a strong dependence on the redox state of the surface. This ultimately stems from the ability of the TiO_2 surface to reductively adsorb O_2 molecules and pass charge from the Au cluster to O_{ad} sites.[29,76] Moreover, all the mechanistic pathways show low barriers that are dependent on the redox state. Since only a kinetic analysis will allow us to estimate which of these routes are viable and under which

DOI: 10.1021/jacs.6b04187
J. Am. Chem. Soc. 2016, 138, 10467−10476

reaction conditions, we have built a microkinetic model that includes four distinct features: (i) both adsorbed oxygen species (O_2 or O_{ad}) and the O_b ion can be the oxidative species for CO oxidation; (ii) both the gold cluster perimeter sites and the O_{ad}—Au^+—CO sites can be active for CO oxidation; (iii) we account for the change in the reaction energetics of the redox steps (both O_2 adsorption and CO oxidation) as a function of the oxidation state of the TiO_2 support surface; (iv) since all reactions show small energy barriers, both forward and reverse rates are included.

Table 2 summarizes the data for 10 elementary reaction steps computed from the current DFT models. Two sets of energetics are listed to account for low or high oxidizing conditions. Further, the 10 elementary reaction steps are organized into five distinct catalytic cycles for CO oxidation: (i) Langmuir–Hinshelwood (LH) mechanism, (ii) DMvK mechanism, (iii) the hybrid LM mechanism, (iv) interfacial atomic oxygen (AL) mechanism where the O_2 dissociates first and CO then directly reacts with the O_{ad}, and (v) atomic oxygen to single site mechanism (AS) where O_2 dissociates first, CO comes to form O_{ad}—Au^+—CO and then reacts with O_b. The relationship between these mechanisms and the reaction list in Table 2 is summarized in Figure 3. Note that the energetics for the LH mechanism were obtained from our previous study[29] where O_2* species was used for different oxidation levels. The high oxidation level in that study is different from the high oxidation level in the present one. This does not affect the main conclusions in the microkinetic analysis since the DMvK is dominant at high oxidation levels.

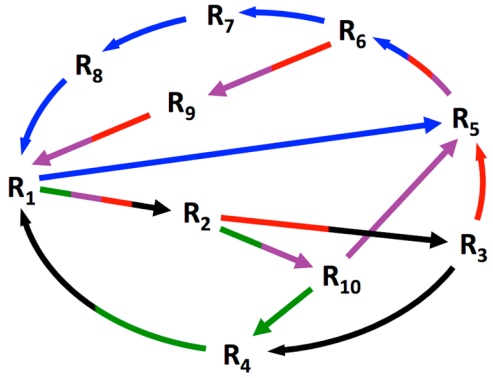

Figure 3. Reactive pathway diagram for possible catalytic mechanisms for CO oxidation on Au/TiO_2 catalyst. Black arrows represents LH mechanism, Blue the DMvK mechanism, Red the LM mechanism, Green the AL mechanism, and Purple the AS mechanism. See text, Table 2 and additional Table S3 for a full description.

In the LH mechanism proposed in previous studies[29,51,56] a CO molecule is initially adsorbed on the gold particle (R1), then O_2 adsorbs at the interface (R2), followed by CO_2 production when the CO and O_2 molecules react, leaving one oxygen atom at the interface (R3). The second CO_2 formation occurs when another CO reacts with O_{ad}, completing the catalytic cycle (R4). In the DMvK mechanism catalysis by O_{ad}—Au^+—CO is feasible under oxidizing condition with elementary steps R1, R5, R6, R7, and R8. The LM catalytic cycle combines a half-cycle of LH and DMvK mechanisms. At first, the CO molecule on the Au cluster reacts with the adsorbed O_2 producing CO_2 (R1, R2, R3), then O_{ad}—Au^+—CO produces another CO_2 by taking O_b (R5, R6), followed by filling O_v with the O_{ad}, completing the catalytic cycle (R9). In the AL mechanism, O_2 dissociates into two O_{ad}, due to a low energy barrier (R2, R10), and each directly reacts with two CO molecules on the Au cluster, producing CO_2 (R1, R4). The AS mechanism includes the O_2 dissociation (R2, R10) as well. When O_{ad}—Au^+—CO is formed (R1, R5) it reacts with O_b to produce CO_2 (R6, R9), followed by occupying the O_v with dissociated oxygen atom.

The complexity of this system inspired us to investigate process kinetics under varying conditions. Microkinetic analyses are performed to estimate the activity of gold nanoparticles as a function of temperature and partial pressure of CO and O_2. Steady-state surface coverages are calculated as the coverage when the rate equations are equal to zero. Then the steady-state rates for the elementary steps are calculated using steady-state surface coverages. These calculations provide a CO_2 production rate for each catalytic cycle. Finally, the ratio of CO_2 production for each catalytic cycle is calculated as the rate of each individual cycle divided by the total CO_2 production rate. Additional details appear in Sections S1 and S5.

Figure 4a shows the ratio (R) of CO_2 production for each catalytic cycle as a function of temperature with partial pressures of P_{O2} = 5 kPa and P_{CO} = 10 kPa. This reveals that the DMvK mechanism is the main contributor of CO_2 production at lower temperatures (between 120 and ~300 K), suggesting that O_{ad}—Au^+—CO is the reactive site in the low temperature range. The coverage evolution of O_{ad} as a function of time supports this assertion (see Figure S1).

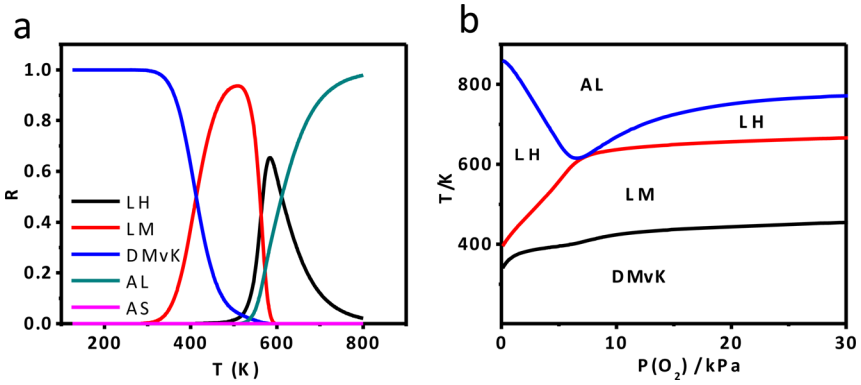

Figure 4. Steady state kinetic results based on microkinetic analysis. (a) The ratio R of CO_2 production from different catalytic cycles at P_{O2} = 5 kP, P_{CO} = 10 kPa. (b) Map of the dominant catalytic pathway (R > 50%) at different temperatures (100–800 K) and O_2 partial pressures (1 kPa ~ 30 kPa).

DOI: 10.1021/jacs.6b04187
J. Am. Chem. Soc. 2016, 138, 10467–10476

Initially, the Au/TiO_2 surface is in a reduced state. O_2 adsorbs at unoccupied interfacial Ti_{5c} sites increasing O_2 coverage (O_2*). Then the CO on the Au cluster reacts with the adsorbed O_2 by overcoming a small barrier (0.32 eV), leading to a slight increase of O_{ad} species. Due to the small energy barrier (0.26 eV), O_{ad}—Au^+—CO forms easily, and interfacial Ti_{5c} sites are gradually saturated by these single site species. This process finally creates a highly oxidized surface at the steady state that favors the DMvK mechanism for CO oxidation. We note that the barrier of the rate-determining step at high oxidation conditions is 0.81 eV, suggesting that measurable reaction rates (~0.1 s^{-1}) can only be distinctly observed at temperatures above 300 K. This is consistent with recent EPR and TAP study by Widmann et al.,[77] reporting that CO oxidation with lattice oxygen is only prevalent at temperatures above 253 K.

At $T \geq 300$ K, the elementary step R9 (O_{ad}* + O_v → O_b) becomes competitive with R7 (O_2 + O_v → O_2*O_v), creating transiently unoccupied Ti_{5c} sites for further O_2 adsorption. This makes the LM the dominant mechanism for CO_2 production at $400 \leq T \leq 550$ K. Under these conditions, the system is still fully oxidized, with all oxygen species (O_2, O_{ad}, and O_b) involved in the catalytic cycle, see Section S1 for detailed rate data. As a result, both the single gold and the cluster perimeter sites become catalytically active.

For temperatures above 500 K, all elementary reactions with an E_a < 1.0 eV occur very fast (>10^2/s). Thus, under oxidized conditions the isolated O_{ad}—Au^+—CO species will quickly react, and generate O_v sites that are quickly filled by O_{ad}. In addition, the reaction rate of elementary step R4 (CO# + O_{ad} * → CO_2 + * + #) is increased very fast (see Table S4), which can quickly remove O_{ad} species. By T > 550 K, these processes will significantly reduce O_{ad}—Au^+—CO formation, leaving a significant number of unoccupied Ti_{5c} sites and creating a low oxidation condition. As a result, the LH mechanism becomes dominant. O_2 dissociation is substantially favored at higher temperatures, which results in the observation of the AL mechanism. The AS mechanism is not observed in the temperature range between 100 and 800 K, because at low temperature O_{ad} sites are all covered by Au—CO species (forming O_{ad}—Au^+—CO) and are not available for CO oxidation; at high temperature the surface is under low oxidation state and O_{ad}—Au^+—CO is not reactive.

Figure 4b displays the dominant (contributing more than 50% of the CO_2 production) catalytic mechanisms under steady state conditions as a function of temperature and partial pressure of O_2. Generally, at a specific P_{O2} the dominant catalytic mechanism changes by the following order DMvK→ LM→ LH → AL as temperature increases. The DMvK mechanism is preferred at low temperatures (<400 K) for all P_{O2}. At low O_2 partial pressures (<8 kPa) the LH mechanism mainly occurs over a relatively broad temperature range (400 to 800 K), while at high O_2 partial pressures (>20 kPa), this mechanism dominates CO_2 production at a narrow temperature range from 650−750 K. Finally, over a wide range of temperatures and pressures at least 2 or 3 mechanistic routes occur simultaneously.

DISCUSSION

Our kinetic model can help reconcile several controversies existing in the gold catalysis literature. At the outset, we note that although the current kinetic model can reasonably represent the apparent activation energies reported in experiments, it fails to reproduce the correct order of reaction rates for two reasons: (1) catalysts are always prepared under moist conditions or pretreated with a reducing H_2 atmosphere, leading to unavoidable existence of surface hydroxyls, whereas our model only uses the oxygen species coverage to reflect the surface oxidation state; and (2) the correlation between oxidation states and activation energies suggest that a meanfield microkinetic model may not be sufficient to capture the local variation in reactivity. This will lead to an underestimation of the apparent activation entropy, and affect pre-exponential factor estimation. For example, in recent studies[78,79] water was found to enhance CO_2 formation rates because OH^- and H_2O species change the mechanistic steps and introduce new intermediate species. A detailed Kinetic Monte Carlo (KMC) simulation, similar to the work by Stamatakis et al.,[25] may effectively reduce this underestimation but this is not the purpose of the current work. Here we aim to demonstrate how active sites, reactive species and mechanisms are dependent on operating conditions and show that, qualitatively, this model can provide some insights into the existing experimental observations and contraversies.

First, there is a lively debate on the nature of the catalytic active site. Many STM and FTIR experiments have suggested that gold catalysts experience large morphological changes at the cluster/oxide interface during CO oxidation.[26,37,80−82] Perimeter sites between gold particles and the support are generally reported to be the active center for CO oxidation,[35] while several recent studies have suggested that the atomically dispersed Au sites on the oxide support are in fact the active ones.[83−86] Specially, Flytzani−Stephanopoulos et al.,[87] suggested that dispersing catalytic gold as widely as possible will maximize activity. In the present work, we provide an explanation of how atomic Au sites arise dynamically on the oxide supported gold nanoparticles under reaction conditions. The O_{ad}—Au^+—CO sites are not fully isolated from the nanoparticle but remain adjacent and can be dynamically available as conditions allow. Thus, ensemble measurement techniques or those with low time/spatial resolution may not be able to differentiate them from perimeter sites. Moreover, which site is actually active depends on the reaction conditions.

Only a few kinetic studies[26,52,74,88−92] have been performed to obtain apparent activation energies for CO oxidation on Au/TiO_2; the values vary from 0.2−0.8 eV with the notable observation that the highest activation energies are obtained under highly oxidizing conditions. See the summarized information in Table S6. There is neither consensus nor a consistent understanding of why there is such a wide variance.[93] Given our results, we postulate that apparent activation energies strongly depend on the catalyst preparation method and the level of oxidation of the catalyst/support under operando conditions. Most studies point out that Au/TiO_2 nanocatalysts exhibit a high activity for CO oxidation with a barrier of ~0.2−0.4 eV at low temperatures.[26,52,74,92] However, it was also reported that catalysts often deactivated very rapidly within only 1−2 h. Goodman et al.,[74,92] attributed the deactivation to Au cluster agglomeration, but the estimated activation energy only changed by 0.1 eV, when the size of the Au cluster changed from 3 to 6 nm. Moreover, Behm et al.,[90] pointed out that size effects could not be the main deactivation culprit due to the observed small changes in particle size. Recently, Green et al.,[52] also observed that the reaction rate of CO oxidation declined within 1 h on CO-saturated Au/TiO_2 catalysts (P_{O2} = 1 Torr and T = 120 K), and attributed the deactivation to the difficulty of CO diffusion to the interface

DOI: 10.1021/jacs.6b04187
J. Am. Chem. Soc. 2016, 138, 10467−10476

(reported diffusion barriers of 0.5−0.7 eV). However, our AIMD simulations show the Au—CO unit diffusing throughout the gold cluster with an estimated energy barrier of only 0.23 eV (see Figure S5), such that CO diffusion is likely not the reason behind the observed catalyst deactivation.

On the basis of our microkinetic analysis, we determine that it is the O_{ad}—Au^+—CO species at the interface that hinders CO oxidation at low temperature and low O_2 partial pressures. Under typical surface science experiment conditions the surface is initially under reducing conditions and the low P_{O2} does not allow for a high coverage of O_{ad}. As such, CO oxidation will proceed via the LH mechanism. From our kinetic model the apparent activation energy is estimated to be only ∼0.3 eV under such conditions. However, this is not sustainable due to the fast formation of O_{ad}—Au^+—CO at the interfacial area. High coverage of O_{ad}—Au^+—CO will eventually lead to a high oxidation state of the surface where the DMvK mechanism dominates. Under these conditions, the apparent activation energy is estimated to be ∼0.8 eV and thus will have reduced activity at low temperatures.

Furthermore, Haruta et al.,[26] and Fujitani et al.,[23] reported two temperature regimes for CO oxidation on Au/TiO_2 catalysts: one with a low apparent activation energy of ∼0.3 eV at low temperatures, and another with almost no activation energy (∼0.02 eV) at increased temperatures (above 300−400 K). Moreover, Fujitani et al., pointed out that the CO_2 formation rates at 400 K remained nearly constant regardless of the mean gold particle diameter, and suggested that the active sites were newly created on the gold−metal surface at high temperatures.[23] Interestingly, the calculated Arrhenius plots based on our microkinetic modeling confirm the observed phenomena, as shown in Figure 5. At P_{O2} = 5 kPa and P_{CO} = 10 kPa, the plot exhibits a clear slope over the low temperature range (T < 550 K) that becomes almost flat at high temperature range (T > 550 K). This is a result of the change in the dominant reaction mechanism from LM to LH and AL, as seen in Figure 4a. As noted in Table S6, the experimental kinetics are typically measured either under low oxidation conditions or in the presence of water, which is believed to significantly improve the activity of CO oxidation. We thus performed microkinetic analyses under low and high oxidizing conditions. For the former, we assume that the catalyst remains partially reduced, and we limit the coverage of oxygen species to be lower than the saturation levels, but allow for the formation of O_{ad}—Au^+—CO. For both low and high oxidation models, the simulated kinetics show two regimes for CO oxidation see Figure 5. The apparent activation energy varies with reduction level such that low values are obtained for low oxidizing conditions and high values obtained for high oxidizing conditions. We note that some experimental kinetics for CO oxidation are obtained under UHV conditions[92,94] and thus are not taken under steady state, which are not relevant to our microkinetic analysis. However, due to the low oxygen chemical potential under UHV condition, the surface is easily remains in a low oxidized state, which will make the LH mechanism favorable at low temperature. This is consistent with our prediction that under low oxidizing condition, the LH mechanisms is dominant and has a small apparent activation barrier (0.29 eV). Validation of the current findings can be achiveved by steady state kinetic measurements where the reduction level (O_{ad} coverage) of the surface is carefully monitored and controlled.

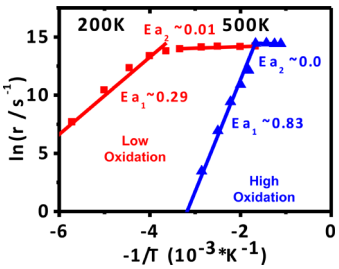

Figure 5. Arrhenius plots of the total CO_2 production rate at $P(O_2)$ = 5 kPa, $P(CO)$ = 10 kPa.

CONCLUSIONS

In summary, we performed a detailed mechanistic investigation at the atomic level of CO oxidation catalyzed by Au/TiO_2 with AIMD simulations and microkinetic modeling. We identified a novel single gold atom Mars van Krevelen (DMvK) and hybrid single atom/nanoparticle mechanisms at the cluster/oxide interface. Under reactive conditions, CO adsorption leads to the formation of single Au sites that are strongly linked to surface O_{ad}. However, unlike catalysis by an isolated Au-adatoms considered previously, after the catalytic cycle is completed, the single gold atom returns to the gold nanoparticle indicating that this specific active site exists only in operando. Depending on reaction conditions, this species can lead to potential catalyst deactivation. We summarized five possible catalytic routes for CO oxidation that occur on Au/TiO_2 nanocatalysts. Microkinetic analyses show that the dominant catalytic mechanisms, activated oxygen species, and catalytic active sites strongly depend on both temperature and oxygen partial pressure. This is a result of the fact that the thermodynamics as well as the reaction energy barriers depend on the level of oxidation of the support material/catalyst which is a feature unique to reducible oxide supports. This underscores an important general principle that reactive conditions modulate not only the catalytic pathways but also the active sites and highlights the fact that catalysis is a dynamic process where the catalyst adapts its configuration to suit reaction conditions to optimally perform a reaction.

ASSOCIATED CONTENT

Supporting Information

The Supporting Information is available free of charge on the ACS Publications website at DOI: 10.1021/jacs.6b04187.

Movie of AIMD trajectories showing O_{ad}—Au^+—CO formation (MPG)

Movie of AIMD trajectories showing O_{ad}—Au^+—CO formation (MPG)

Details of microkinetic analysis, side views of MD snapshots, dynamic behavior of Au—CO, the mobility and stability of O_{ad}—Au^+—CO at the interface, oxygen vacancy under gold cluster, and summarized experimental kinetics for CO oxidation on Au/TiO_2 (PDF)

AUTHOR INFORMATION

Corresponding Author

*roger.rousseau@pnnl.gov

Notes

The authors declare no competing financial interest.

DOI: 10.1021/jacs.6b04187
J. Am. Chem. Soc. 2016, 138, 10467−10476

■ ACKNOWLEDGMENTS

This work was supported by the US Department of Energy, Office of Basic Energy Sciences, Division of Chemical Sciences, Geosciences & Biosciences and performed at the Pacific Northwest National Laboratory (PNNL). PNNL is a multi-program national laboratory operated for Department of Energy by Battelle. Computational resources were provided at W. R. Wiley Environmental Molecular Science Laboratory (EMSL), a national scientific user facility sponsored by the Department of Energy's Office of Biological and Environmental Research located at PNNL and the National Energy Research Scientific Computing Center (NERSC) at Lawrence Berkeley National Laboratory.

■ REFERENCES

(1) Taylor, H. S. *Proc. R. Soc. London, Ser. A* **1925**, *108*, 105.
(2) Tao, F.; Crozier, P. A. *Chem. Rev.* **2016**, *116*, 3487.
(3) Bordiga, S.; Groppo, E.; Agostini, G.; van Bokhoven, J. A.; Lamberti, C. *Chem. Rev.* **2013**, *113*, 1736.
(4) Bañares, M. A. *Catal. Today* **2005**, *100*, 71.
(5) Bañares, M. A. *Adv. Mater.* **2011**, *23*, 5293.
(6) Frenkel, A. I.; Cason, M. W.; Elsen, A.; Jung, U.; Small, M. W.; Nuzzo, R. G.; Vila, F. D.; Rehr, J. J.; Stach, E. A.; Yang, J. C. *J. Vac. Sci. Technol., A* **2014**, *32*, 020801.
(7) Mondloch, J. E.; Bayram, E.; Finke, R. G. *J. Mol. Catal. A: Chem.* **2012**, *355*, 1.
(8) Vajda, S.; Winans, R. E.; Elam, J. W.; Lee, B.; Pellin, M. J.; Seifert, S.; Tikhonov, G. Y.; Tomczyk, N. A. *Top. Catal.* **2006**, *39*, 161.
(9) Laoufi, I.; Saint-Lager, M.-C.; Lazzari, R.; Jupille, J.; Robach, O.; Garaudée, S.; Cabailh, G.; Dolle, P.; Cruguel, H.; Bailly, A. *J. Phys. Chem. C* **2011**, *115*, 4673.
(10) Roldan Cuenya, B. *Acc. Chem. Res.* **2013**, *46*, 1682.
(11) Flytzani-Stephanopoulos, M. *Acc. Chem. Res.* **2014**, *47*, 783.
(12) Yang, M.; Allard, L. F.; Flytzani-Stephanopoulos, M. *J. Am. Chem. Soc.* **2013**, *135*, 3768.
(13) Ding, K.; Gulec, A.; Johnson, A. M.; Schweitzer, N. M.; Stucky, G. D.; Marks, L. D.; Stair, P. C. *Science* **2015**, *350*, 189.
(14) Qiao, B.; Wang, A.; Yang, X.; Allard, L. F.; Jiang, Z.; Cui, Y.; Liu, J.; Li, J.; Zhang, T. *Nat. Chem.* **2011**, *3*, 634.
(15) Stephens, I. E. L.; Elias, J. S.; Shao-Horn, Y. *Science* **2015**, *350*, 164.
(16) Herzing, A. A.; Kiely, C. J.; Carley, A. F.; Landon, P.; Hutchings, G. J. *Science* **2008**, *321*, 1331.
(17) Yang, X.-F.; Wang, A.; Qiao, B.; Li, J.; Liu, J.; Zhang, T. *Acc. Chem. Res.* **2013**, *46*, 1740.
(18) Zhang, S.; Nguyen, L.; Liang, J.-X.; Shan, J.; Liu, J.; Frenkel, A. I.; Patlolla, A.; Huang, W.; Li, J.; Tao, F. *Nat. Commun.* **2015**, *6*, 7938.
(19) Wang, J.; McEntee, M.; Tang, W.; Neurock, M.; Baddorf, A. P.; Maksymovych, P.; Yates, J. T. *J. Am. Chem. Soc.* **2016**, *138*, 1518.
(20) Gao, M.-R.; Liang, J.-X.; Zheng, Y.-R.; Xu, Y.-F.; Jiang, J.; Gao, Q.; Li, J.; Yu, S.-H. *Nat. Commun.* **2015**, *6*, 5982.
(21) Liang, J.-X.; Lin, J.; Yang, X.-F.; Wang, A.-Q.; Qiao, B.-T.; Liu, J.; Zhang, T.; Li, J. *J. Phys. Chem. C* **2014**, *118*, 21945.
(22) Ghosh, P.; Farnesi Camellone, M.; Fabris, S. *J. Phys. Chem. Lett.* **2013**, *4*, 2256.
(23) Fujitani, T.; Nakamura, I. *Angew. Chem., Int. Ed.* **2011**, *50*, 10144.
(24) van Santen, R. A.; Ghouri, M. M.; Shetty, S.; Hensen, E. M. *Catal. Sci. Technol.* **2011**, *1*, 891.
(25) Stamatakis, M.; Christiansen, M. A.; Vlachos, D. G.; Mpourmpakis, G. *Nano Lett.* **2012**, *12*, 3621.
(26) Haruta, M. *Gold Bull.* **2004**, *37*, 27.
(27) Negreiros, F. R.; Camellone, M. F.; Fabris, S. *J. Phys. Chem. C* **2015**, *119*, 21567.
(28) Camellone, M. F.; Kowalski, P. M.; Marx, D. *Phys. Rev. B: Condens. Matter Mater. Phys.* **2011**, *84*, 035413.
(29) Wang, Y.-G.; Yoon, Y.; Glezakou, V.-A.; Li, J.; Rousseau, R. *J. Am. Chem. Soc.* **2013**, *135*, 10673.
(30) Wang, Y.-G.; Mei, D.; Li, J.; Rousseau, R. *J. Phys. Chem. C* **2013**, *117*, 23082.
(31) Wang, Y.-G.; Mei, D.; Glezakou, V.-A.; Li, J.; Rousseau, R. *Nat. Commun.* **2015**, *6*, 6511.
(32) Lee, M.-S.; McGrail, B. P.; Rousseau, R.; Glezakou, V.-A. *Sci. Rep.* **2015**, *5*, 14857.
(33) Rousseau, R.; Schenter, G. K.; Fulton, J. L.; Linehan, J. C.; Engelhard, M. H.; Autrey, T. *J. Am. Chem. Soc.* **2009**, *131*, 10516.
(34) Liu, J.-C.; Tang, Y.; Chang, C.-R.; Wang, Y.-G.; Li, J. *ACS Catal.* **2016**, *6*, 2525.
(35) Takei, T.; Akita, T.; Nakamura, I.; Fujitani, T.; Okumura, M.; Okazaki, K.; Huang, J.; Ishida, T.; Haruta, M. *Adv. Catal.* **2012**, *55*, 1.
(36) Friend, C. M.; Hashmi, A. S. K. *Acc. Chem. Res.* **2014**, *47*, 729.
(37) Freakley, S. J.; He, Q.; Kiely, C. J.; Hutchings, G. J. *Catal. Lett.* **2015**, *145*, 71.
(38) Chrétien, S.; Metiu, H. *J. Chem. Phys.* **2007**, *126*, 104701.
(39) Chrétien, S.; Metiu, H. *J. Chem. Phys.* **2007**, *127*, 084704.
(40) Chrétien, S.; Metiu, H. *J. Chem. Phys.* **2007**, *127*, 244708.
(41) Widmann, D.; Behm, R. J. *Acc. Chem. Res.* **2014**, *47*, 740.
(42) Green, I. X.; Tang, W.; Neurock, M.; Yates, J. T., Jr *Acc. Chem. Res.* **2014**, *47*, 805.
(43) Chrétien, S.; Metiu, H. *J. Chem. Phys.* **2008**, *129*, 074705.
(44) Chrétien, S.; Metiu, H. *J. Chem. Phys.* **2008**, *128*, 044714.
(45) Stiehl, J. D.; Kim, T. S.; McClure, S. M.; Mullins, C. B. *J. Am. Chem. Soc.* **2004**, *126*, 13574.
(46) Stiehl, J. D.; Kim, T. S.; McClure, S. M.; Mullins, C. B. *J. Am. Chem. Soc.* **2004**, *126*, 1606.
(47) Li, L.; Zeng, X. C. *J. Am. Chem. Soc.* **2014**, *136*, 15857.
(48) Liu, Z.-P.; Gong, X.-Q.; Kohanoff, J.; Sanchez, C.; Hu, P. *Phys. Rev. Lett.* **2003**, *91*, 266102.
(49) Koga, H.; Tada, K.; Okumura, M. *J. Phys. Chem. C* **2015**, *119*, 25907.
(50) Cai, Q.; Wang, X.; Wang, J.-g. *J. Phys. Chem. C* **2013**, *117*, 21331.
(51) Molina, L.; Rasmussen, M.; Hammer, B. *J. Chem. Phys.* **2004**, *120*, 7673.
(52) Green, I. X.; Tang, W.; Neurock, M.; Yates, J. T. *Science* **2011**, *333*, 736.
(53) Widmann, D.; Behm, R. J. *Angew. Chem., Int. Ed.* **2011**, *50*, 10241.
(54) Liu, L. M.; McAllister, B.; Ye, H. Q.; Hu, P. *J. Am. Chem. Soc.* **2006**, *128*, 4017.
(55) Remediakis, I. N.; Lopez, N.; Nørskov, J. K. *Angew. Chem.* **2005**, *117*, 1858.
(56) Wang, J.; Hammer, B. *Top. Catal.* **2007**, *44*, 49.
(57) Wang, J.; Hammer, B. *Phys. Rev. Lett.* **2006**, *97*, 136107.
(58) Hvolbæk, B.; Janssens, T. V.; Clausen, B. S.; Falsig, H.; Christensen, C. H.; Nørskov, J. K. *Nano Today* **2007**, *2*, 14.
(59) Liu, Z.-P.; Gong, X.-Q.; Kohanoff, J.; Sanchez, C.; Hu, P. *Phys. Rev. Lett.* **2003**, *91*, 266102.
(60) Duan, Z.; Henkelman, G. *ACS Catal.* **2015**, *5*, 1589.
(61) VandeVondele, J.; Krack, M.; Mohamed, F.; Parrinello, M.; Chassaing, T.; Hutter, J. *Comput. Phys. Commun.* **2005**, *167*, 103.
(62) Perdew, J. P.; Burke, K.; Ernzerhof, M. *Phys. Rev. Lett.* **1996**, *77*, 3865.
(63) VandeVondele, J.; Hutter, J. *J. Chem. Phys.* **2007**, *127*, 114105.
(64) Goedecker, S.; Teter, M.; Hutter, J. *Phys. Rev. B: Condens. Matter Mater. Phys.* **1996**, *54*, 1703.
(65) Henkelman, G.; Uberuaga, B. P.; Jónsson, H. *J. Chem. Phys.* **2000**, *113*, 9901.
(66) Reuter, K.; Scheffler, M. *Phys. Rev. B: Condens. Matter Mater. Phys.* **2001**, *65*, 035406.
(67) Fan, C.; Zhu, Y.-A.; Yang, M.-L.; Sui, Z.-J.; Zhou, X.-G.; Chen, D. *Ind. Eng. Chem. Res.* **2015**, *54*, 5901.
(68) Psofogiannakis, G.; St-Amant, A.; Ternan, M. *J. Phys. Chem. B* **2006**, *110*, 24593.

DOI: 10.1021/jacs.6b04187
J. Am. Chem. Soc. 2016, 138, 10467−10476

(69) Cai, Q. X.; Wang, J. G.; Wang, Y. G.; Mei, D. *AIChE J.* **2015**, *61*, 3812.
(70) Filot, I. A.; Broos, R. J.; van Rijn, J. P.; van Heugten, G. J.; van Santen, R. A.; Hensen, E. J. *ACS Catal.* **2015**, *5*, 5453.
(71) Raphulu, M.; McPherson, J.; Van der Lingen, E.; Anderson, J.; Scurrell, M. *Gold Bull.* **2010**, *43*, 21.
(72) Hutchings, G. *Nat. Chem.* **2009**, *1*, 584.
(73) Freakley, S. J.; He, Q.; Kiely, C. J.; Hutchings, G. J. *Catal. Lett.* **2015**, *145*, 71.
(74) Meier, D. C.; Lai, X.; Goodman, D. W. In *Surface Chemistry and Catalysis*; Springer: New York, 2002; p 147.
(75) Vilhelmsen, L. B.; Hammer, B. *ACS Catal.* **2014**, *4*, 1626.
(76) Yoon, Y.; Wang, Y.-G.; Rousseau, R.; Glezakou, V.-A. *ACS Catal.* **2015**, *5*, 1764.
(77) Widmann, D.; Krautsieder, A.; Walter, P.; Brückner, A.; Behm, R. J. *ACS Catal.* **2016**, *6*, 5005.
(78) Fujitani, T.; Nakamura, I.; Haruta, M. *Catal. Lett.* **2014**, *144*, 1475.
(79) Saavedra, J.; Doan, H. A.; Pursell, C. J.; Grabow, L. C.; Chandler, B. D. *Science* **2014**, *345*, 1599.
(80) Hrbek, J.; Hoffmann, F. M.; Park, J. B.; Liu, P.; Stacchiola, D.; Hoo, Y. S.; Ma, S.; Nambu, A.; Rodriguez, J. A.; White, M. G. *J. Am. Chem. Soc.* **2008**, *130*, 17272.
(81) Kolmakov, A.; Goodman, D. *Surf. Sci.* **2001**, *490*, L597.
(82) Saint-Lager, M.-C.; Laoufi, I.; Bailly, A. *Faraday Discuss.* **2013**, *162*, 179.
(83) Li, X.-N.; Yuan, Z.; He, S.-G. *J. Am. Chem. Soc.* **2014**, *136*, 3617.
(84) Wang, C.; Yang, M.; Flytzani-Stephanopoulos, M. *AIChE J.* **2016**, *62*, 429.
(85) Qiao, B.; Liu, J.; Wang, Y.-G.; Lin, Q.; Liu, X.; Wang, A.; Li, J.; Zhang, T.; Liu, J. *ACS Catal.* **2015**, *5*, 6249.
(86) Li, Z.-Y.; Yuan, Z.; Li, X.-N.; Zhao, Y.-X.; He, S.-G. *J. Am. Chem. Soc.* **2014**, *136*, 14307.
(87) Yang, M.; Li, S.; Wang, Y.; Herron, J. A.; Xu, Y.; Allard, L. F.; Lee, S.; Huang, J.; Mavrikakis, M.; Flytzani-Stephanopoulos, M. *Science* **2014**, *346*, 1498.
(88) Bamwenda, G. R.; Tsubota, S.; Nakamura, T.; Haruta, M. *Catal. Lett.* **1997**, *44*, 83.
(89) Long, C. G.; Gilbertson, J. D.; Vijayaraghavan, G.; Stevenson, K. J.; Pursell, C. J.; Chandler, B. D. *J. Am. Chem. Soc.* **2008**, *130*, 10103.
(90) Denkwitz, Y.; Zhao, Z.; Hörmann, U.; Kaiser, U.; Plzak, V.; Behm, R. *J. Catal.* **2007**, *251*, 363.
(91) Green, I. X.; Tang, W.; McEntee, M.; Neurock, M.; Yates, J. T., Jr *J. Am. Chem. Soc.* **2012**, *134*, 12717.
(92) Valden, M.; Pak, S.; Lai, X.; Goodman, D. *Catal. Lett.* **1998**, *56*, 7.
(93) Aguilar-Guerrero, V.; Gates, B. C. *Catal. Lett.* **2009**, *130*, 108.
(94) Bondzie, V. A.; Parker, S. C.; Campbell, C. T. *Catal. Lett.* **1999**, *63*, 143.

DOI: 10.1021/jacs.6b04187
J. Am. Chem. Soc. 2016, 138, 10467−10476